

## Robust inverse identification of piezoelectric and dielectric effective behaviors of a bonded patch to a composite plate

Ayech Benjeddou<sup>\*1</sup>, Mohsen Hamdi<sup>2</sup> and Samir Ghanmi<sup>2</sup>

<sup>1</sup>*Institut Supérieur de Mécanique de Paris, 93400 Saint-Ouen, France*

<sup>2</sup>*Institut Préparatoire aux Etudes d'Ingénieurs de Nabeul, 8000 Nabeul, Tunisia*

(Received May 9, 2013, Revised June 22, 2013, Accepted June 30, 2013)

**Abstract.** Piezoelectric and dielectric behaviors of a piezoceramic patch adhesively centered on a carbon composite plate are identified using a robust multi-objective optimization procedure. For this purpose, the patch piezoelectric stress coupling and blocked dielectric constants are automatically evaluated for a wide frequency range and for the different identifiable behaviors. Latters' symmetry conditions are coded in the design plans serving for response surface methodology-based sensitivity analysis and meta-modeling. The identified constants result from the measured and computed open-circuit frequencies deviations minimization by a genetic algorithm that uses meta-model estimated frequencies. Present investigations show that the bonded piezoceramic patch has effective three-dimensional (3D) orthotropic piezoelectric and dielectric behaviors. Besides, the sensitivity analysis indicates that four constants, from eight, dominate the 3D orthotropic behavior, and that the analyses can be reduced to the electromechanically coupled modes only; therefore, in this case, and if only the dominated parameters are optimized while the others keep their nominal values, the resulting piezoelectric and dielectric behaviors are found to be transverse-isotropic. These results can help designing piezoceramics smart composites for various applications like noise, vibration, shape, and health control.

**Keywords:** finite element-experimental vibration-based mixed inverse identification; multi-objective optimization; piezoelectric effective behavior; dielectric effective behavior; piezoceramic patch; CFRP composite plate

### 1. Introduction

Piezoceramic patches are nowadays the most used actuators and sensors for smart structures applications. In particular, they are very well suited for integration into multilayer fiber reinforced composites that are widely used in modern aeronautic and space constructions. Nevertheless, the piezoceramics electromechanical effective behavior, once integrated into their host composites, is not yet well understood; despite this, only few works exist on this topic (Araujo *et al.* 2010).

Early in the last decade, a first contribution to piezoceramics electromechanical properties inverse identification concerned in-plane piezoelectric stress coupling and blocked transverse relative dielectric constants of PZT-4 piezoceramic layers surface-bonded to a free graphite/epoxy composite plate; this was reached through analytical sensitivities-based gradient optimization of

---

\*Corresponding author, Professor, E-mail: [benjeddou@supmeca.fr](mailto:benjeddou@supmeca.fr)

finite element (FE)-targeted (simulated) frequency weighted squared relative deviations for 12 modes (Araujo *et al.* 2002). A two-dimensional (2D) equivalent single-layer (ESL) third-order shear deformation theory (TSDT)-based quadratic (8 nodes quadrangular) plate FE was proposed for the corresponding simulations. This pioneer work had some shortcomings that concern the piezoelectric stress coupling constants which were not plane stress – reduced as it should be, and the free-vibration problem which was obtained after the element-wise electric degrees of freedom (DOFs) static condensation without considering *a priori* the physical equipotential (EP) conditions on the piezoelectric layers' electrodes. Hence, the solved problems correspond always to an open-circuit (OC) one even for the short-circuit (SC) case that is used for the piezoelectric layers elastic constants identification. Nevertheless, this work (Araujo *et al.* 2002) can be considered as a reference for the three-step (analysis) inverse identification procedure for the identification of the elastic constants of the host structure (bare structure analysis) and bonded piezoelectric layers (SC equipped structure analysis) and the latter's coupling and dielectric constants (OC equipped structure analysis). It's worth noticing here that the optimized transverse shear moduli and piezoelectric stress coupling constants did not correlate well with corresponding target values; deviations were beyond 11%, in particular for the transverse shear modulus  $G_{23}$  which was found 3.4 times lower than the target value.

Later in the same decade, the previous work (Araujo *et al.* 2002) above mentioned shortcomings (absence of stress coupling constants plane-stress reduction, EP conditions enforcement and use of experimental data) have been handled and the gradient optimization procedure has been compared to an artificial neural network (ANN)-based one (Araujo *et al.* 2006). Here, 15 modes of a 12 layers (with lamination sequence  $[0/90/45/-45/0/90]_S$ ) unidirectional (UD) carbon (T300)/Epoxy plate surface-bonded on one side with 9 equally spaced PZT PIC151 patches have been considered. From the conducted analyses' results, preference has been given to the gradient optimization. Unfortunately, in this work, while the piezoelectric strain coupling constants have been linked to the identified plane stress-reduced in-plane stress coupling ones, the blocked transverse dielectric constant was not identified. Remarkably, here also, that the optimized transverse shear moduli, in particular  $G_{23}$  for the plate and  $G_{13}$  for the patch, did not correlate well with the corresponding target values; in contrary, this time, the plane stress-reduced piezoelectric stress coupling constants correlated relatively well with target values.

The inverse identification procedure as in (Araujo *et al.* 2002, 2006) has been later applied to two (A and B) 16 layers (with laminate stacking sequence  $[90/45/0/-45]_{2S}$ ) UD carbon fiber reinforced polymer (CFRP material IMS/977-2) composite plates with four pairs of co-localized PZT PIC255 piezoceramic patches (Araujo *et al.* 2009a); the latter were optimally located on the plates' both sides using a genetic algorithm (GA) that maximizes the weighted sum of the plates first 6 active modal loss factors following linearly decreasing weights with the modes index. Here, 13 modes were retained for the plates and patches elastic and piezoelectric parameters identifications, and an in-house layer-wise (LW) first-order shear deformation theory (FSDT)-based plate FE was used for the numerical simulations. It's worth noticing that the composite plates and piezoceramic patches' behaviors were found to be orthotropic (*orth*), while their manufacturers considered them as transverse quasi-isotropic (QI) and transverse-isotropic (TI), respectively. Besides, the identified effective parameters were very different from those provided (partially) by the manufacturers. Based on another similar work (Araujo *et al.* 2009b) that used earlier benchmarks and models as in (Araujo *et al.* 2006), the identified constants values' differences and behaviors asymmetries were attributed to the patches-to-plate adhesive layers which properties are uncertain and their modeling was not possible within the proposed 2D

identification procedure.

The three-step inverse identification procedure, as outlined in (Araujo *et al.* 2002, 2006, 2009a, b), was recently used (Montemurro *et al.* 2012) for the identification (simulations only) of the elastic and piezoelectric properties of 9 PZT-5H piezoceramic patches bonded on one side of a 12 layers UD carbon/epoxy (T300/5280) composite plate in a similar configuration and stacking sequence to those in (Araujo *et al.* 2006, 2009b). Therefore, the elastic behavior of the plate was *a priori* assumed transverse isotropic (plane 2–3) with known properties, while that of the patches was assumed orthotropic; however, their behavior was identified as transverse isotropic (plane 1–2). The claimed added values include the use of commercial software quadratic 3D (20 nodes) and 2D shell FE for modeling the host plate and patches, respectively, and the GA-based optimization for minimizing a non-weighted sum of frequencies' squared deviations for 30 modes; the GA and commercial software were coupled via an interface so that a FE analysis is called by the GA each optimization's iteration. Noticeable bad correlations concern here the identified longitudinal Young's modulus ( $E_3$ ) and strain piezoelectric coupling constant  $d_{33}$  which deviations were beyond 10% of the corresponding target values. The invoked reason is that these parameters' effects on the plate's frequencies are negligible. The shortcomings of this work concern the patches dielectric properties which were not identified following the same justifications as in (Araujo *et al.* 2006, 2009a,b), the coupling of the GA and FE iterative analysis which leads to a high-cost optimization process, and the unrealistic (non-measurable) high number of modes used for the identification.

From the above literature analysis, it can be summarized that the vibration-based inverse identification procedure that uses various optimization algorithms (gradient, ANN, GA) in conjunction with 2D ESL or LW FE, either for the host and the patches (Araujo *et al.* 2002, 2006, 2009 a,b) or for the latter only (Montemurro *et al.* 2012), led always to an, or *a priori* assumed (Montemurro *et al.* 2012a), orthotropic piezoelectric behavior of the patches, while their fundamental behavior is transverse isotropic. While considering 3D FE modeling and behavior of the patches, with related elastic constants full definiteness relations, is an enhancement (Montemurro *et al.* 2012) to earlier works (Araujo *et al.* 2002, 2006, 2009a,b), assuming *a priori* orthotropic behavior, known elastic data of the host and its 2D shell modeling together with integration of full 3D FE analysis within the GA optimization process are rather drawbacks. Besides, except once and for the transverse dielectric constant only (Araujo *et al.* 2002), the dielectric behavior was not identified in (Araujo *et al.* 2006, 2009a,b, Montemurro *et al.* 2012) where the manufacturer's value was used.

Recently, the three-step inverse identification procedure (Araujo *et al.* 2009a) has been revisited (Hamdi *et al.* 2010, 2012) using the experimentally identified frequencies, among other modal properties (Chevallier and Benjeddou 2009), as inputs; the benchmark consists of a composite plate cut as plate C, like plates A and B of (Araujo *et al.* 2009a), from a 16 layers CFRP large panel and surface-centered adhesively on one of its sides with a PZT PIC255 piezoceramic patch. The originalities of this new contribution to this research field concern the use of: (i) 3D quadratic (20 nodes) FE for modeling both the host plate and the patch in order to avoid the models kinematics assumptions influence which is not negligible as shown in (Wesolowski and Barkanov 2012), (ii) the use of the response surface methodology (RSM) for the sensitivity analysis in order to investigate computational gains from potential design parameters reduction by keeping only the dominant ones, and for meta-modeling, (iii) the use of the RSM-induced polynomial meta-models, instead of FE, for saving computation time during the non-sorting GA (NSGA II) optimization process, (iv) frequencies multiple (multi-objective) deviations and not the latter's modal sum (single-objective), (v) uncertain initial elastic, piezoelectric and dielectric

composite and piezoceramic materials constants through a realistic variation margin of +/-20% as informed by manufacturers websites in order to reach a robust identification, (vi) all materials' behaviors possibilities (orthotropic, transverse quasi-isotropic, and transverse isotropic) for identifying the materials effective behaviors without making *a priori* assumptions. These features are to be considered as the main differences with the literature state of the art (Araujo *et al.* 2002, 2006, 2009a,b, 2010, Montemurro *et al.* 2012). The use of the resulting robust multi-objective three-step inverse identification procedure, extending that used earlier for adaptive structures electro-mechanical updating (Hamdi *et al.* 2013), to above described CFRP plate/PZT PIC255 patch benchmark has led, in a first step, to a transverse-isotropic behavior of the composite plate and, in a second step, to a quasi-isotropic behavior of the PZT PIC255 patch; the remaining third step, for identifying the patch piezoelectric and dielectric behaviors, is then the focus of the present work.

In the following, the identifiable piezoelectric and dielectric behaviors of the piezoceramic patch material are first described in order to highlight their symmetry relations to be coded within the plans of simulation designs; then, the robust multi-objective inverse identification procedure is described; next, the latter's application to the identifications of the patch piezoelectric and dielectric behaviors is detailed; finally, this work summary and related conclusions are given as a closure.

## 2. Identifiable piezoelectric and dielectric behaviors

The general orthotropic 3D converse and direct piezoelectric constitutive equations for a polarization along the material axis 3 can be written in the *e-form* as, respectively

$$\begin{Bmatrix} T_1 \\ T_2 \\ T_3 \\ T_4 \\ T_5 \\ T_6 \end{Bmatrix} = \begin{bmatrix} c_{11}^E & c_{12}^E & c_{13}^E & 0 & 0 & 0 \\ c_{12}^E & c_{22}^E & c_{23}^E & 0 & 0 & 0 \\ c_{13}^E & c_{23}^E & c_{33}^E & 0 & 0 & 0 \\ 0 & 0 & 0 & c_{44}^E & 0 & 0 \\ 0 & 0 & 0 & 0 & c_{55}^E & 0 \\ 0 & 0 & 0 & 0 & 0 & c_{66}^E \end{bmatrix} \begin{Bmatrix} S_1 \\ S_2 \\ S_3 \\ S_4 \\ S_5 \\ S_6 \end{Bmatrix} - \begin{bmatrix} 0 & 0 & e_{31} \\ 0 & 0 & e_{32} \\ 0 & 0 & e_{33} \\ 0 & e_{24} & 0 \\ e_{15} & 0 & 0 \\ 0 & 0 & 0 \end{bmatrix} \begin{Bmatrix} E_1 \\ E_2 \\ E_3 \end{Bmatrix} \quad (1)$$

$$\begin{Bmatrix} D_1 \\ D_2 \\ D_3 \end{Bmatrix} = \begin{bmatrix} 0 & 0 & 0 & 0 & e_{15} & 0 \\ 0 & 0 & 0 & e_{24} & 0 & 0 \\ e_{31} & e_{32} & e_{33} & 0 & 0 & 0 \end{bmatrix} \begin{Bmatrix} S_1 \\ S_2 \\ S_3 \\ S_4 \\ S_5 \\ S_6 \end{Bmatrix} + \begin{bmatrix} \epsilon_{11}^S & 0 & 0 \\ 0 & \epsilon_{22}^S & 0 \\ 0 & 0 & \epsilon_{33}^S \end{bmatrix} \begin{Bmatrix} E_1 \\ E_2 \\ E_3 \end{Bmatrix}$$

Where,  $T_p$ ,  $S_q$ ,  $D_i$ ,  $E_k$  ( $p, q = 1, \dots, 6$ ;  $i, k = 1, 2, 3$ ) are the stress, strain, electric displacement and electric field components, respectively, while  $c_{pq}^E$ ,  $e_{pk}$  and  $\epsilon_{ii}^S$  are, respectively, the *shorted* (at constant electric field) elastic stiffness, stress piezoelectric coupling, and *blocked* (at constant

strain) dielectric constants.

The presence of electrodes on upper and lower in-plane surfaces of a piezoelectric patch results in a through-the-thickness *dominant* electric field so that Eq. (1) reduce to

$$\begin{Bmatrix} T_1 \\ T_2 \\ T_3 \\ T_4 \\ T_5 \\ T_6 \end{Bmatrix} = \begin{bmatrix} c_{11}^E & c_{12}^E & c_{13}^E & 0 & 0 & 0 \\ c_{12}^E & c_{22}^E & c_{23}^E & 0 & 0 & 0 \\ c_{13}^E & c_{23}^E & c_{33}^E & 0 & 0 & 0 \\ \hline 0 & 0 & 0 & c_{44}^E & 0 & 0 \\ 0 & 0 & 0 & 0 & c_{55}^E & 0 \\ 0 & 0 & 0 & 0 & 0 & c_{66}^E \end{bmatrix} \begin{Bmatrix} S_1 \\ S_2 \\ S_3 \\ S_4 \\ S_5 \\ S_6 \end{Bmatrix} - \begin{bmatrix} 0 & 0 & e_{31} \\ 0 & 0 & e_{32} \\ 0 & 0 & e_{33} \\ \hline 0 & e_{24} & 0 \\ e_{15} & 0 & 0 \\ 0 & 0 & 0 \end{bmatrix} \begin{Bmatrix} 0 \\ 0 \\ E_3 \end{Bmatrix} \quad (2)$$

$$\begin{Bmatrix} D_1 \\ D_2 \\ D_3 \end{Bmatrix} = \begin{bmatrix} 0 & 0 & 0 & 0 & e_{15} & 0 \\ 0 & 0 & 0 & e_{24} & 0 & 0 \\ e_{31} & e_{32} & e_{33} & 0 & 0 & 0 \end{bmatrix} \begin{Bmatrix} S_1 \\ S_2 \\ S_3 \\ S_4 \\ S_5 \\ S_6 \end{Bmatrix} + \begin{bmatrix} \epsilon_{11}^S & 0 & 0 \\ 0 & \epsilon_{22}^S & 0 \\ 0 & 0 & \epsilon_{33}^S \end{bmatrix} \begin{Bmatrix} 0 \\ 0 \\ E_3 \end{Bmatrix}$$

Hence, when the patch electrodes are *shorted* the dominant electric field can be approximately nil so that Eq. (2) first line reduces to the following pure elastic constitutive equation

$$\begin{Bmatrix} T_1 \\ T_2 \\ T_3 \\ T_4 \\ T_5 \\ T_6 \end{Bmatrix} = \begin{bmatrix} c_{11}^E & c_{12}^E & c_{13}^E & 0 & 0 & 0 \\ c_{12}^E & c_{22}^E & c_{23}^E & 0 & 0 & 0 \\ c_{13}^E & c_{23}^E & c_{33}^E & 0 & 0 & 0 \\ \hline 0 & 0 & 0 & c_{44}^E & 0 & 0 \\ 0 & 0 & 0 & 0 & c_{55}^E & 0 \\ 0 & 0 & 0 & 0 & 0 & c_{66}^E \end{bmatrix} \begin{Bmatrix} S_1 \\ S_2 \\ S_3 \\ S_4 \\ S_5 \\ S_6 \end{Bmatrix} \quad (3)$$

Therefore, in order to identify the *elastic* behavior (Eq. (3)) of a bonded or integrated patch, it is necessary to consider *shorted* (SC) electrodes during testing and simulation, while *open* (OC) electrodes need to be considered for identifying the piezoelectric (matrix  $[e]$ ) and dielectric (matrix  $[\epsilon^S]$ ) behaviors; in this case, the elastic (matrix  $[c^E]$ ) behavior needs to be *a priori* known or identified; the latter also requires that the host structure elastic (matrix  $[c]$ ) behavior needs to be *a priori* known or identified. This explains why a three-step identification procedure is necessary to identify the host elastic (step 1: without patch) behavior and the bonded/integrated patch elastic (step 2: with SC patch) and piezoelectric/dielectric (step 3: with OC patch) behaviors.

Thickness polarized piezoelectric patches are generally very thin so that they approximately do not suffer transverse shear stresses ( $T_4 = T_5 = 0$ ); consequently, Eq. (2) reduce further to these ones

$$\begin{Bmatrix} T_1 \\ T_2 \\ T_3 \\ T_6 \end{Bmatrix} = \begin{bmatrix} c_{11}^E & c_{12}^E & c_{13}^E & 0 \\ c_{12}^E & c_{22}^E & c_{23}^E & 0 \\ c_{13}^E & c_{23}^E & c_{33}^E & 0 \\ 0 & 0 & 0 & c_{66}^E \end{bmatrix} \begin{Bmatrix} S_1 \\ S_2 \\ S_3 \\ S_6 \end{Bmatrix} - \begin{Bmatrix} e_{31} \\ e_{32} \\ e_{33} \\ 0 \end{Bmatrix} E_3 \quad (4)$$

$$D_3 = \langle e_{31} \quad e_{32} \quad e_{33} \quad 0 \rangle \begin{Bmatrix} S_1 \\ S_2 \\ S_3 \\ S_6 \end{Bmatrix} + \epsilon_{33}^S E_3$$

Also, thin piezoelectric patches do not suffer thickness stress so that, using the third line of Eq. (4) together with  $T_3=0$  and after substituting back resulting  $S_3 = -(c_{13}^E S_1 + c_{23}^E S_2 - e_{33} E_3) / c_{33}^E$  relation, the following *plane-stress reduced* constitutive equations are obtained

$$\begin{Bmatrix} T_1 \\ T_2 \\ T_6 \end{Bmatrix} = \begin{bmatrix} \bar{c}_{11}^E & \bar{c}_{12}^E & 0 \\ \bar{c}_{12}^E & \bar{c}_{22}^E & 0 \\ 0 & 0 & c_{66}^E \end{bmatrix} \begin{Bmatrix} S_1 \\ S_2 \\ S_6 \end{Bmatrix} - \begin{Bmatrix} \bar{e}_{31} \\ \bar{e}_{32} \\ 0 \end{Bmatrix} E_3 \quad (5)$$

$$D_3 = \langle \bar{e}_{31} \quad \bar{e}_{32} \quad 0 \rangle \begin{Bmatrix} S_1 \\ S_2 \\ S_6 \end{Bmatrix} + \bar{\epsilon}_{33}^S E_3$$

With  $\bar{c}_{\alpha\beta}^E = c_{\alpha\beta}^E - c_{\beta 3}^E \frac{c_{13}^E}{c_{33}^E}$ ,  $\bar{e}_{3\alpha} = e_{3\alpha} - e_{33} \frac{c_{\alpha 3}^E}{c_{33}^E}$  ( $\alpha, \beta = 1, 2$ ) and  $\bar{\epsilon}_{33}^S = \epsilon_{33}^S + \frac{(e_{33})^2}{c_{33}^E}$  being the *plane stress-reduced* elastic, stress piezoelectric coupling and blocked transverse dielectric constants; together with  $c_{pp}^E$  ( $p = 4, 5, 6$ ), these constants are those that a plate/shell 2D model with transverse shear handling can identify at most; while the corresponding elastic engineering constants can be accessed, there is no way to access to the corresponding original stress piezoelectric coupling and blocked dielectric constants; besides, the transverse normal Young's modulus and the two transverse (major or minor) Poisson's ratios, as well as the transverse normal (longitudinal) stress piezoelectric coupling and the two in-plane blocked dielectric constants remain unidentifiable by a plate/shell 2D model. Hence, the identified engineering constants using such models remain insufficient for conducting 3D simulations. For the latter purpose, it is then necessary to consider 3D modeling of both the host structure and the patch.

As stated above, Eqs. (1)-(5) characterize an electromechanically (elastic, piezoelectric and dielectric) orthotropic behavior; hence, possibly identifiable *effective* piezoelectric and dielectric behaviors of a bonded or integrated piezoceramic patch are *orthotropic*. In the 3D case, as in Eq. (1), 8 parameters, grouped into the design vector  $\mathbf{x}_{orth}$ , are to be identified

$$e_{31}, e_{32}, e_{33}, e_{15}, e_{24}, \epsilon_{11}^s, \epsilon_{22}^s, \epsilon_{33}^s \quad (6)$$

Other possible identifiable effective piezoelectric and dielectric behaviors of a bonded or integrated piezoceramic patch are *transverse–isotropic* when these symmetry relations hold

$$e_{32} = e_{31}, e_{33}, e_{24} = e_{15}, \epsilon_{22}^s = \epsilon_{11}^s, \epsilon_{33}^s \quad (7)$$

Hence, in this case, only 5 parameters, grouped into the design vector  $\mathbf{x}_{TI}$ , are to be identified

$$e_{31}, e_{33}, e_{15}, \epsilon_{11}^s, \epsilon_{33}^s \quad (8)$$

It's worth noticing that, together with the right elastic symmetry relations, those of Eq. (7) can be used to derive Eqs. (1)-(5) for full electromechanical TI behavior. Besides, from (8), it should be recalled that  $(e_{31}, \epsilon_{33}^s)$  characterize the *transverse* (or  $e_{31}$ ),  $(e_{33}, \epsilon_{33}^s)$  the *longitudinal* (or  $e_{33}$ ), and  $(e_{15}, \epsilon_{11}^s)$  the shear (or  $e_{15}$ ) response of the piezoceramic patch; hence, as shown above, only the transverse response is considered by a plate/shell 2D model–based identification. Therefore, the three piezoelectric coupling responses are present naturally in full 3D model–based identifications. Finally, worthy to notice that the TI symmetry relations, as in Eq. (7), are here coded within the plan of simulation designs for TI sensitivity analysis and RSM meta–modeling.

### 3. Robust multi-objective identification methodology

The proposed three–step identification procedure is illustrated in Fig. 1. Each step could be analyzed independently from the earlier(s) if the latter's corresponding material(s) behavior(s) was (were) identified (known) *a priori*; that is, for example, identifying the piezoelectric and dielectric behaviors of a bonded/integrated patch requires *a priori* identifying (or knowing) its elastic behavior and that of the host structure. For the present investigations, which focus on the bonded patch piezoelectric and dielectric behaviors (step 3), the *elastic* behavior of the host CFRP composite *plate* was identified as *transverse–isotropic* (step 1: cf. Hamdi *et al.* 2010) and that of the bonded *patch* as *transverse quasi–isotropic* (step 2: cf. Hamdi *et al.* 2012).

The minimization of the frequency relative deviations for the materials behaviours' parameters robust multi–objective identification follows the flowchart of Fig. 2. First, for an investigated effective behaviour, the 3D initial piezoelectric and dielectric parameters of the piezoceramic patch are complemented from the manufacturer's generic data using material behaviour symmetry relations and assuming the remaining parameter(s) as detailed in Chevallier *et al.* (2008), while the patch and host elastic parameters are those identified in Hamdi *et al.* (2010) (transverse isotropic elastic effective behaviour of the composite plate) and Hamdi *et al.* (2012) (quasi–isotropic elastic effective behaviour of the bonded patch), respectively; then, using ANSYS® FE commercial software, 3D simulations are conducted according to a numerical designs complete factorial plan of size  $m^n$  for  $n$  design variables and  $m$  levels (here two levels of +/-20% uncertainties following manufacturers data information) each; next, sensitivity analysis can be conducted for influential parameters assessment in order to investigate potential reduction of the design parameters' number in order to decrease the size of the simulation designs plan, hence to save computations time. Meta–modelling is then conducted using the RSM with full second–order polynomials (Myers 2002); finally, experimental frequencies, taken from Chevallier and Benjeddou (2009), are used as

inputs of the NSGA II–based (Deb *et al.* 2002) multi–objective optimization (Deb 2007) and as references for residual errors evaluation serving for behaviours identification. Notice that compared to Hamdi *et al.* (2013), where NSGA has been used, here NSGA II is retained for the optimization. The coupling of the NSGA II and meta–models is shown in Fig. 3.

The RSM–induced meta–models require their validation using statistical measures such as:

- The *determination* factor  $R^2$  that should be as close as possible to unity ( $0 < R^2 \leq 1$ , Batzmaz and Tunali 2003) and should give information about the models fitting goodness

$$R^2 = 1 - \frac{\sum_{i=1}^n (\hat{y}_i - y_i)^2}{\sum_{i=1}^n (y_i - \bar{y}_i)^2} \quad (9)$$

Where,  $y_i$ ,  $\hat{y}_i$ ,  $\bar{y}_i$  are the exact response, estimated one, and mean of the exact responses.

- The *mean square error* (MSE) which, in order to satisfy the 6 sigma criterion, should not overpass this value 0.09028 (Battaglia and Maynard 1996); the MSE is defined as

$$MSE = \frac{\sum_{i=1}^m (y_i - \hat{y}_i)^2}{\bar{y}_i \times \sigma_{y_i}^2} \quad (10)$$

With,  $\sigma_{y_i}$  being the exact responses standard deviation.

The NSGA–II parameters are fixed after a parametric analysis as: selection probability  $P_s = 0.8$ , crossing probability  $P_c = 0.5$ , mutation probability  $P_m = 0.01$ , initial population size of 30, and generation number of 50.

#### 4. Piezoelectric and dielectric behaviors identifications

The proposed robust multi–objective optimization–based inverse identification procedure is now applied to the piezoelectric and dielectric behaviors characterization of a PZT PIC255 patch of dimensions 50 mm, 25 mm, 0.3 mm along the frame axes x, y, z, respectively, and centered on a 16–ply laminated CFRP composite plate of stacking sequence  $[90/45/0/-45]_{2S}$  and dimensions 200.3 mm, 300 mm and 4.2 mm along x, y, z. The plate and patch elastic behaviors have been identified previously as TI (Hamdi *et al.* 2010) and QI (Hamdi *et al.* 2012), respectively, and the corresponding elastic engineering constants are recalled in Table 1 together with the patch nominal (initial) piezoelectric and dielectric parameters. Their measured mass densities are, respectively, 1521 Kg/m<sup>3</sup> and 7720.3 Kg/m<sup>3</sup>. The adaptive plate was tested in a free (wire–hanged) configuration.

The piezoelectric adaptive composite structure (composite plate + piezoceramic patch) OC free vibration modal properties are extracted for a given piezoelectric and dielectric effective behaviour of the patch using the block Lanczos algorithm within ANSYS<sup>®</sup> FE commercial software; materials initial data of Table 1 and in–plane mesh (Table 2), corresponding to the 9 geometric partitions of Fig. 4, are used. For this purpose, the elastic quadratic (20 nodes) SOLID191 FE is used for modelling the host laminated composite plate, and the fully coupled piezoelectric

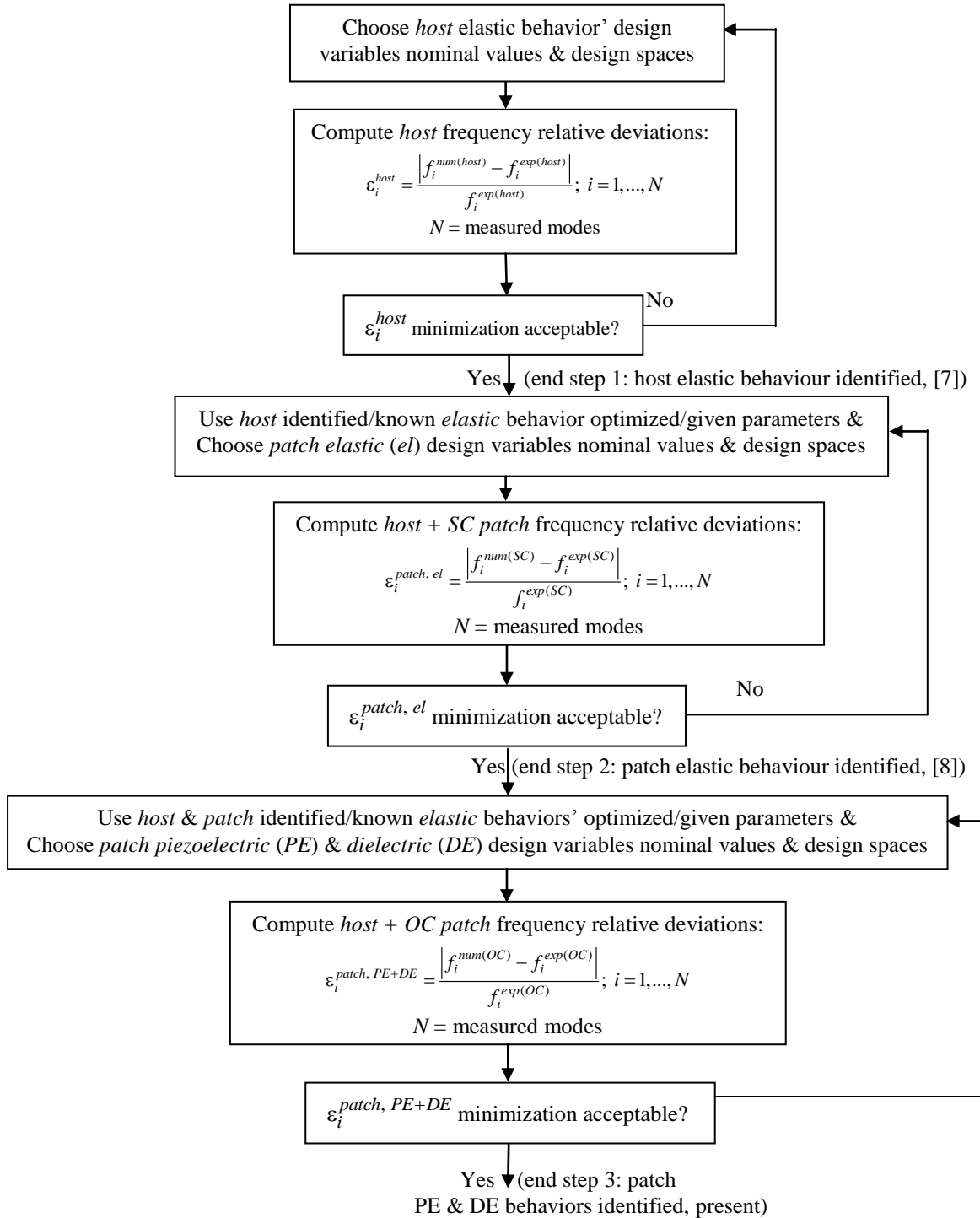


Fig. 1 Three-step frequency minimization-based materials behaviors' robust multi-objective identification ([7] Hamdi *et al.* 2010, [8] Hamdi *et al.* 2012)

quadratic (20 nodes) SOLID226 FE is used for modelling the patch. Using only 1 FE in each of the plate and patch thickness, the FE model has 4200 FEs and 28280 nodes.

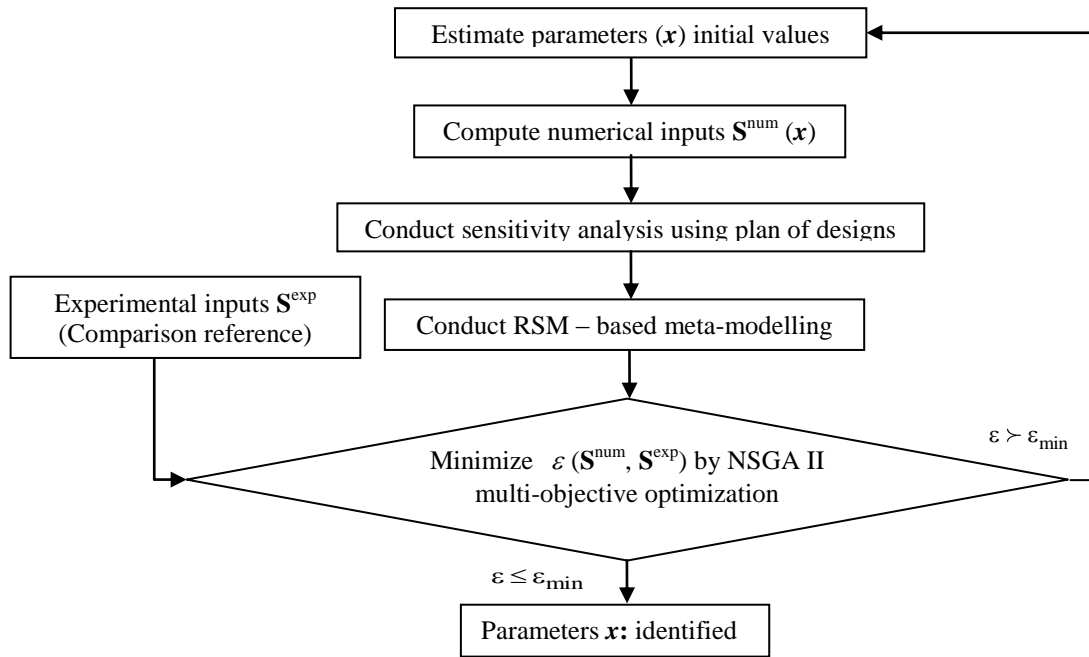


Fig. 2 Proposed behaviour/parameters' robust multi-objective identification methodology

Table 1 Optimized elastic and nominal piezoelectric and dielectric engineering constants

CFRP plate	$Y_1$	$Y_2$	$Y_3$	$G_{12}$	$G_{13}$	$G_{23}$	$\nu_{12}$	$\nu_{13}$	$\nu_{23}$	
elastic moduli (GPa)	121.04	11.51	11.51	5.68	5.68	3.64	0.38	0.38	0.58	
Patch	$Y_1^E$	$Y_2^E$	$Y_3^E$	$G_{12}^E$	$G_{13}^E$	$G_{23}^E$	$\nu_{12}^E$	$\nu_{13}^E$	$\nu_{23}^E$	
SC elastic moduli (GPa)	49.68	49.68	51.80	18.8	16.8	16.8	0.26	0.35	0.35	
stress piezoelectric (C/m <sup>2</sup> ) & blocked dielectric (nF/m)	$e_{31}$	$e_{32}$	$e_{33}$	$e_{15}$	$e_{24}$		$\epsilon_{22}^S$	$\epsilon_{22}^S$	$\epsilon_{33}^S$	$\epsilon^0 (\times e^{-3})$
nominal (initial) values	-7.25	-7.25	14.41	11.57	11.57	8.245	8.245	7.122	8.854	

Table 2 FE mesh of the piezoelectric adaptive composite plate domains partition

Parameter	$L_1$	$L_2$	$L_3$	$B_1$	$B_2$	$B_3$
Dimension (mm)	137.5	25	137.5	71.15	50	75.15
Number of FE	20	25	20	15	25	15
Size of a FE (mm)	6.875	1	6.875	5.01	2	5.01

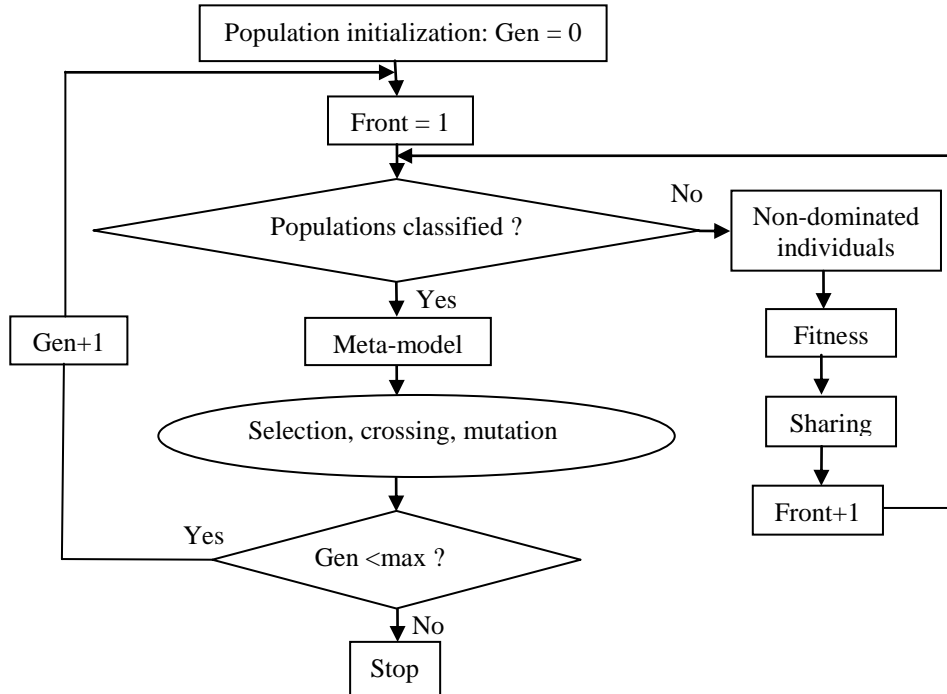


Fig. 3 NSGA II and meta-model combination

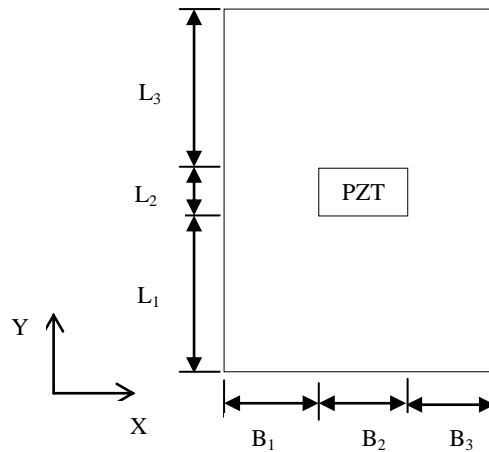


Fig. 4 Position of the patch on the plate and domains partition for the FE mesh generation

Optimization references are made to the measured first eight SC and OC frequencies, and squared effective (structural) modal electromechanical coupling coefficients (EMCC) of the smart plate (composite host + PZT PIC255 patch) that are post-treated using the following definition

(Benjeddou 2009, 2010)

$$K^2 = \frac{f_{oc}^2 - f_{sc}^2}{f_{sc}^2} \quad (11)$$

From the experimental results, recalled from Chevallier and Benjeddou (2009) in Table 3, it can be noticed that only four modes (2, 4, 7, 8) are electromechanically coupled (Fig. 7 of Appendix A).

Table 3 Reference experimental SC and OC frequencies, and post treated modal effective EMCC values

Mode (type)	1 (1,1)	2 (0,2)	3 (1,2)	4 (2,0)	5 (2,1)	6 (0,3)	7 (1,3)	8 (2,2)
$f_{sc}$ (Hz)	229.6	311.3	553.8	580.6	725.0	888.8	1067.0	1161.5
$f_{oc}$ (Hz)	229.6	311.5	553.8	581.8	725.0	888.8	1067.3	1164.0
$K^2$ (%)	0	0.128	0	0.412	0	0	0.056	0.429

Since the patch piezoelectric and dielectric effective behaviors are unknown *a priori*, identifiable orthotropic and transverse–isotropic ones are analysed hereafter before and after corresponding sensitivities analyses.

Table 4 Orthotropic RSM meta–models and statistical measures of the first 8 OC modes

OC frequencies RSM–induced polynomial meta–models	$R^2$	MSE
$\hat{f}_1 = 230.77 - 0.005625x_1 - 0.005625x_2 - 0.009375x_3$ $- 1.62 \times 10^{-14}x_4 + 5.55 \times 10^{-15}x_5 - 3.7 \times 10^{-14}x_6 - 9.75 \times 10^{-14}x_7 - 6.2 \times 10^{-4}x_8$	0.97	0.02746
$\hat{f}_2 = 310.76 + 0.064375x_1 - 0.1325x_2 - 0.06875x_3$ $+ 0.00125x_4 - 4.22 \times 10^{-15}x_5 - 4.91 \times 10^{-14}x_6 - 1.27 \times 10^{-13}x_7 - 0.001875x_8$	0.96	0.04382
$\hat{f}_3 = 556.29$	-	-
$\hat{f}_4 = 585.37 - 0.59391x_1 + 0.088906x_2 - 0.49016x_3$ $+ 0.0014063x_4 + 0.00078125x_5 - 3.15 \times 10^{-14}x_6 - 2.36 \times 10^{-13}x_7 - 0.013281x_8$	0.97	0.02924
$\hat{f}_5 = 724.21$	-	-
$\hat{f}_6 = 889.18$	-	-
$\hat{f}_7 = 1076 - 0.28125x_1 - 0.08125x_2 - 0.35625x_3$ $+ 6.75 \times 10^{-14}x_4 - 2.84 \times 10^{-14}x_5 - 8.70 \times 10^{-14}x_6 - 5.99 \times 10^{-13}x_7 - 0.00625x_8$	0.98	0.01779
$\hat{f}_8 = 1172.4 - 0.57187x_1 - 0.040625x_2 - 0.59063x_3$ $+ 0.003125x_4 - 8.7 \times 10^{-4}x_5 - 1.81 \times 10^{-13}x_6 - 3.35 \times 10^{-13}x_7 - 0.015625x_8$	0.98	0.02236

4.1 Identifiable piezoelectric and dielectric effective behaviors analyses

Consider that, in general, the patch may have orthotropic piezoelectric and dielectric effective behaviors; the latter have 8 design parameters, as defined in Eq. (6), having two levels, min (-1) and max (+1), and varying in the design space of +/-20% around their nominal values given in Table 1. This leads to a designs complete factorial plan of 2<sup>8</sup>=256 simulations to be conducted under OC electrodes of the patch. Applying a second-order RSM to each of the 8 OC frequencies provides the corresponding meta-models given in Table 4.

Table 4 shows, first, that all meta-models are valid statistically since they satisfy the statistical measures thresholds as in Eqs. (9) and (10); then, it indicates that the 3<sup>rd</sup>, 5<sup>th</sup> and 6<sup>th</sup> frequencies are constant; i.e., they are not influenced by varying the piezoelectric and dielectric design parameters. This interesting result can be explained by the fact that these modes are in fact electromechanically uncoupled (see Table 3). Next, from the powers of the terms multiplying the design parameters, it is expected that the transverse shear (x<sub>4</sub>, x<sub>5</sub>) and in-plane dielectric (x<sub>6</sub>, x<sub>7</sub>) constants shall not be much influential on the four (2, 4, 7, 8) electromechanically coupled modes; this can be explained by the thinness of the plate and patch. Hence, the shear piezoelectric responses, characterized by these parameters, are here negligible. Finally, the first mode appears here slightly coupled in contrary to the corresponding experimentally nil EMCC; this result can be explained by the fact that a low EMCC may not be measurable via SC/OC vibrations (Chevallier and Benjeddou 2009).

Consider now a transverse isotropic initial behavior for which symmetry relations (7) hold so that the number of design parameters reduces to the 5 ones given in Eq. (8). Using the same two levels and design space as for the orthotropic case, the designs complete factorial plan reduces here to only 2<sup>5</sup>=32 simulations (see Table 17 in Appendix B) to be conducted also under OC electrodes of the patch. Applying again a second-order RSM to each of the 8 OC frequencies provides the corresponding meta-models given in Table 5; here also, the latter shows that the meta-models are valid statistically and that only the electromechanically coupled modes are influenced by the variation of the design parameters. Besides, the coupled modes are not much influenced by the transverse shear piezoelectric response characteristic design parameters (x<sub>3</sub>, x<sub>4</sub>).

Table 5 Transverse isotropic RSM meta-models and statistical measures of the first 8 OC modes

OC frequencies RSM-induced polynomial meta-models	R <sup>2</sup>	MSE
$\hat{f}_1 = 230.77 - 0.01125x_1 - 0.00875x_2 + 6.28 \times 10^{-15}x_3 - 2.01 \times 10^{-14}x_4 - 0.00125x_5$	0.97	0.02870
$\hat{f}_2 = 310.75 - 0.068125x_1 - 0.065625x_2 + 0.000625x_3 - 3.39 \times 10^{-14}x_4 - 0.001875x_5$	0.98	0.01576
$\hat{f}_3 = 556.29$	-	-
$\hat{f}_4 = 585.35 - 0.505x_1 - 0.48375x_2 + 0.00125x_3 - 6.78 \times 10^{-14}x_4 - 0.01375x_5$	0.98	0.01675
$\hat{f}_5 = 724.21$	-	-
$\hat{f}_6 = 889.18$	-	-
$\hat{f}_7 = 1076 - 0.3625x_1 - 0.3625x_2 + 5.02 \times 10^{-15}x_3 - 1.81 \times 10^{-13}x_4 - 0.0125x_5$	0.98	0.01585
$\hat{f}_8 = 1172.4 - 0.6125x_1 - 0.5875x_2 + 1.51 \times 10^{-14}x_3 - 7.03 \times 10^{-14}x_4 - 0.0125x_5$	0.98	0.01733

Applying the robust multi-objective inverse identification procedure 3<sup>rd</sup> step (Fig. 1) with

meta-models (Table 4 for the orthotropic case and Table 5 for the transverse – isotropic one)–estimated OC frequencies, instead of FE ones, during NSGA II optimization (Fig. 3), provides the design parameters of Table 6 and corresponding variations with regards to (w.r.t.) nominal ones. It can be noticed that some parameters reach the limit range of the allowed 20% variation; however, this limit was not changed because realistic, and not mathematical only, variation is targeted. The resulting OC frequencies and related residual errors w.r.t experimental ones are given in Table 7. It can be noticed that these residual errors cannot help distinguishing the two behaviors; hence, squared effective modal EMCC are post-treated as shown in Table 8. Here, when compared to the experimental EMCC values, the optimized ones indicate that the piezoelectric and dielectric effective behaviors of the bonded patch are *orthotropic*.

Table 6 Design parameters after robust multi-objective optimization-based identification

Stress piezoelectric (C/m <sup>2</sup> ) & blocked dielectric (nF/m)	e <sub>31</sub>	e <sub>32</sub>	e <sub>33</sub>	e <sub>24</sub>	e <sub>15</sub>	ε <sub>11</sub> <sup>S</sup>	ε <sub>22</sub> <sup>S</sup>	ε <sub>33</sub> <sup>S</sup>
	Orthotropic behavior	-8.7	-8.7	17.29	13.84	12.21	9.04	9.89
% variation w.r.t. nominal	20	20	20	19.61	5.53	9.68	20	20
Transverse isotropic behavior	-8.7	-8.7	17.29	11.58	11.58	7.24	7.24	7.00
% variation w.r.t. nominal	20	20	20	0.12	0.12	-12.22	-12.22	-1.66

Table 7 OC frequencies after robust multi-objective optimization-based identification

Mode (type)	1 (1,1)	2 (0,2)	3 (1,2)	4 (2,0)	5 (2,1)	6 (0,3)	7 (1,3)	8 (2,2)
$f_{OC,orth}$ (Hz)	230.77	310.74	556.29	585.27	724.21	889.18	1075.9	1172.3
% error	0.509	-0.243	0.449	<b>0.596</b>	-0.108	0.042	0.805	0.713
$f_{OC,TI}$ (Hz)	230.77	310.75	556.29	585.28	724.21	889.18	1075.9	1172.3
% error	0.509	<b>-0.240</b>	0.449	0.598	-0.108	0.042	0.805	0.713

Table 8 Post-treated EMCC values after robust multi-objective optimization-based identification

Mode (type)	1 (1,1)	2 (0,2)	3 (1,2)	4 (2,0)	5 (2,1)	6 (0,3)	7 (1,3)	8 (2,2)
$K_{orth}^2$ (%)	0.069	<b>0.284</b>	0	<b>1.151</b>	0	0	0.466	0.651
$K_{TI}^2$ (%)	0.069	0.290	0	1.155	0	0	0.466	0.651

#### 4.2 A priori sensitivity-based identifiable effective behaviors analyses

The sensitivity analysis aims, first, to measure the influence of the design variables (here patches' stress piezoelectric coupling and blocked dielectric constants) and their interactions on the observed response (OC frequencies) variations, so that non-influential variables can be dropped. It is based on previous complete factorial plans used for orthotropic (256 simulation designs), and transverse-isotropic (32 simulation designs) patch piezoelectric and dielectric effective behaviors identification. The design parameters' effects on the 8 OC frequencies are computed using the classical analysis of variance (ANOVA) statistical approach. Hence, for a design variable experiment, a given parameter's effect is the result of the scalar cross product of 256 (orthotropic) or 32 (transverse isotropic)–sized vectors containing the non-dimensional design

variable levels (-1, +1) and corresponding simulations designs' OC frequencies (Hz); for all sensitivity analyses, design parameters effects on the OC frequencies are then in Hz.

The orthotropic 8 design parameters effects on the first 8 OC frequencies are shown in Fig. 5.

As expected from corresponding meta-models (Table 4) discussion, the latter figure shows that the most influential parameters are  $e_{31}$ ,  $e_{32}$ ,  $e_{33}$  and  $\epsilon_{33}^s$  (corresponding to  $x_1$ ,  $x_2$ ,  $x_3$  and  $x_8$  of Table 4, respectively) that characterize the extension (transverse and longitudinal) piezoelectric responses; also, only the four electromechanically coupled modes (2, 4, 7, 8) are influenced by the latter.

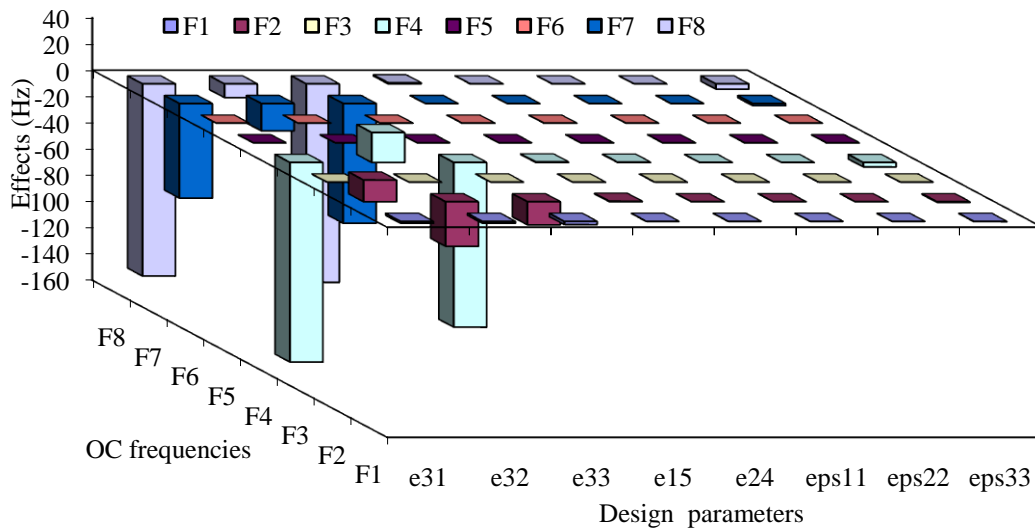


Fig. 5 Orthotropic behaviour 8 design parameters effects on the 8 OC frequencies

The transverse-isotropic 5 design parameters' influence on the 8 OC frequencies is shown in Fig. 6. Here also, as expected from corresponding meta-models (Table 5) discussion, the latter figure shows that  $e_{31} = e_{32}$ ,  $e_{33}$ ,  $\epsilon_{33}^s$  (corresponding to  $x_1$ ,  $x_2$ ,  $x_5$  of Table 5, respectively) are the most influential parameters on the four electromechanically coupled modes (2, 4, 7, 8) only.

Only above 4 orthotropic or 3 transverse-isotropic influent parameters resulting from the sensitivity analyses as in Figs. 5 and 6, respectively, are now retained for the patch piezoelectric and dielectric behaviors identification; this leads, respectively, to simulation designs complete factorial plans of reduced sizes to only  $2^4 = 16$  (Table 18 in Appendix B) and  $2^3 = 8$  (Table 19 in Appendix B), and to the corresponding meta-models given in Table 9 and Table 10. The latter show again that only the four electromechanically coupled modes (2, 4, 7, 8) are affected by the influent parameters variations. Also, Table 9 shows that the first mode is almost uncoupled since the polynomial coefficients powers of the coupling ( $x_1$ ,  $x_2$ ,  $x_3$ ) and dielectric ( $x_4$ ) parameters are low.

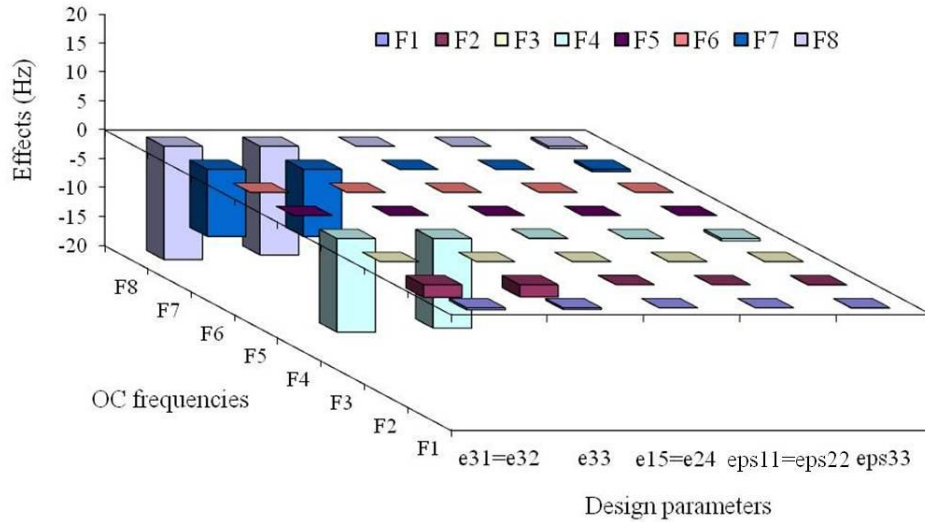


Fig. 6 Transverse isotropic behaviour 5 design parameters effects on the 8 OC frequencies

Table 9 Influent parameters–based orthotropic RSM meta–models and statistical measures

OC frequencies RSM–induced polynomial meta–models	$R^2$	MSE
$\hat{f}_1 = 230.77 - 5.625 \times 10^{-3}x_1 - 5.625 \times 10^{-3}x_2 - 9.375 \times 10^{-3}x_3 - 6.25 \times 10^{-4}x_4$	0.97	0.02585
$\hat{f}_2 = 310.76 + 0.065x_1 - 0.13375x_2 - 0.06875x_3 - 1.25 \times 10^{-3}x_4$	0.96	0.04152
$\hat{f}_3 = 556.29$	-	-
$\hat{f}_4 = 585.37 - 0.59313x_1 + 0.088125x_2 - 0.49063x_3 - 0.013125x_4$	0.97	0.02734
$\hat{f}_5 = 724.21$	-	-
$\hat{f}_6 = 889.18$	-	-
$\hat{f}_7 = 1076 - 0.28125x_1 - 0.08125x_2 - 0.35625x_3 - 6.25 \times 10^{-3}x_4$	0.98	0.01674
$\hat{f}_8 = 1172.4 - 0.56875x_1 - 0.04375x_2 - 0.59375x_3 - 0.01875x_4$	0.98	0.02003

The application of the robust multi–objective inverse identification procedure 3<sup>rd</sup> step (Fig. 1), using the influent (*infl*) design parameters only–based meta–models of Table 9 for the orthotropic and Table 10 for the transverse–isotropic cases during NSGA II optimization (Fig. 3), provides the design parameters of Table 11 and corresponding variations w.r.t. nominal ones. Notice that the non–influential parameters keep their nominal (initial) values during the optimization process and that  $e_{32}=e_{31}$  TI constraint is coded in the corresponding simulation designs plan. Worthy to notice is that only the blocked transverse dielectric constant values differ after the influent parameters orthotropic and TI optimizations.

Table 10 Influential parameters-based transverse isotropic RSM meta-models and statistical measures

OC frequencies RSM-induced polynomial meta-models	R <sup>2</sup>	MSE
$\hat{f}_1 = 230.77 - 0.01125x_1 - 8.75 \times 10^{-3}x_2 - 1.25 \times 10^{-3}x_3$	0.97	0.02593
$\hat{f}_2 = 310.75 - 0.06875x_1 - 0.06625x_2 - 1.25 \times 10^{-3}x_3$	0.98	0.01242
$\hat{f}_3 = 556.29$	-	-
$\hat{f}_4 = 585.35 - 0.505x_1 - 0.4825x_2 - 0.0125x_3$	0.98	0.01513
$\hat{f}_5 = 724.21$	-	-
$\hat{f}_6 = 889.18$	-	-
$\hat{f}_7 = 1076 - 0.3625x_1 - 0.3625x_2 - 0.0125x_3$	0.98	0.01432
$\hat{f}_8 = 1172.4 - 0.6125x_1 - 0.5875x_2 - 0.0125x_3$	0.98	0.01565

Table 11 Influential design parameters-based robust multi-objective optimized behaviors constants

Stress piezoelectric (C/m <sup>2</sup> ) & blocked dielectric (nF/m)	e <sub>31</sub>	e <sub>32</sub>	e <sub>33</sub>	e <sub>15</sub>	e <sub>24</sub>	ε <sub>11</sub> <sup>S</sup>	ε <sub>22</sub> <sup>S</sup>	ε <sub>33</sub> <sup>S</sup>
Orthotropic behavior	-8.7	-8.7	17.29	11.57	11.57	8.245	8.245	8.546
% variation w.r.t. nominal	20	20	20	0	0	0	0	20
Transverse isotropic behavior	-8.7	-8.7	17.29	11.57	11.57	8.245	8.245	<b>8.080</b>
% variation w.r.t. nominal	20	20	20	0	0	0	0	<b>13.45</b>

The OC frequencies and related residual errors w.r.t experimental ones, and resulting squared effective modal EMCC corresponding to the design parameters of Table 11 are given in Table 12 and Table 13, respectively. It can be noticed that, both the frequencies residual errors and optimized EMCC, when compared to their experimental values, indicate that the piezoelectric and dielectric effective behaviors of the bonded patch are still *orthotropic*.

Table 12 Influential parameters-based OC frequencies after robust multi-objective optimization

Mode (type)	1 (1,1)	2 (0,2)	3 (1,2)	4 (2,0)	5 (2,1)	6 (0,3)	7 (1,3)	8 (2,2)
$f_{OC, orth-infl}$ (Hz)	230.77	310.74	556.29	585.27	724.21	889.18	1075.9	1172.3
% error	0.509	-0.244	0.450	<b>0.596</b>	-0.109	0.043	0.806	0.713
$f_{OC, TI-infl}$ (Hz)	230.77	310.74	556.29	585.28	724.21	889.18	1075.9	1172.3
% error	0.509	-0.244	0.450	0.598	-0.109	0.043	0.806	0.713

Table 13 Influential parameters-based EMCC after robust multi-objective optimization

Mode (type)	1 (1,1)	2 (0,2)	3 (1,2)	4 (2,0)	5 (2,1)	6 (0,3)	7 (1,3)	8 (2,2)
$K_{orth-infl}^2$ (%)	0.069	0.284	0	<b>1.151</b>	0	0	0.466	0.651
$K_{TI-infl}^2$ (%)	0.069	0.284	0	1.155	0	0	0.466	0.651

Table 14 Influent design parameters and coupled modes multi-objective optimized behaviors constants

Stress piezoelectric (C/m <sup>2</sup> ) & blocked dielectric (nF/m)	e <sub>31</sub>	e <sub>32</sub>	e <sub>33</sub>	e <sub>15</sub>	e <sub>24</sub>	ε <sub>11</sub> <sup>S</sup>	ε <sub>22</sub> <sup>S</sup>	ε <sub>33</sub> <sup>S</sup>
Orthotropic behavior	-8.7	-5.8	11.53	11.57	11.57	8.245	8.245	5.698
% variation w.r.t. nominal	20	-20	-20	0	0	0	0	-20
Transverse isotropic behavior	-5.8	-5.8	11.53	11.57	11.57	8.245	8.245	<b>7.303</b>
% variation w.r.t. nominal	-20	-20	-20	0	0	0	0	<b>2.55</b>

Table 15 Influent parameters-based OC frequencies after coupled modes multi-objective optimization

Mode (type)	1 (1,1)	2 (0,2)	3 (1,2)	4 (2,0)	5 (2,1)	6 (0,3)	7 (1,3)	8 (2,2)
<i>f</i> <sub>OC-cm, orth-infl</sub> (Hz)	230.78	310.60	556.29	586.75	724.21	889.18	1076.6	1173.7
% error	0.513	-0.288	0.449	0.850	-0.108	0.042	0.871	0.833
<i>f</i> <sub>OC-cm, TI-infl</sub> (Hz)	230.77	310.74	556.29	585.23	724.21	889.18	1075.9	1172.3
% error	<b>0.509</b>	<b>-0.243</b>	0.449	<b>0.589</b>	-0.108	0.042	<b>0.805</b>	<b>0.713</b>

In a final analysis, consider now the computationally very interesting and practical case of optimizing the orthotropic (4) and transverse-isotropic (3) influent parameters for the electro-mechanically coupled modes (*cm*) only. Therefore, the complete factorial plans are those of previous analysis, but the multi-objective optimization process is here half-reduced by using only modes 2, 4, 7, 8 meta-models. Corresponding optimized influent design parameters, resulting OC frequencies residual errors, and post-treated squared effective modal EMCC results are provided in Table 14, Table 15 and Table 16, respectively. From the latter, it can be concluded that the bonded patch piezoelectric and dielectric behaviors are now *transverse isotropic*. Here, even the OC frequencies residual errors are decisive (bold values are the closest to the experimental ones).

Table 16 Influent parameters-based EMCC after coupled modes multi-objective optimization

Mode (type)	1 (1,1)	2 (0,2)	3 (1,2)	4 (2,0)	5 (2,1)	6 (0,3)	7 (1,3)	8 (2,2)
<i>K</i> <sup>2</sup> <sub>orth-infl</sub> (%)	0.078	<b>0.193</b>	0	1.663	0	0	0.597	0.892
<i>K</i> <sup>2</sup> <sub>TI-infl</sub> (%)	<b>0.069</b>	0.284	0	<b>1.137</b>	0	0	<b>0.466</b>	<b>0.651</b>

## 5. Conclusions

Piezoelectric and dielectric effective behaviors of a centrally bonded piezoceramic patch on a laminated CFRP composite plate were identified using a robust multi-objective mixed numerical-experimental optimization. The latter combines response surface methodology (RSM)-based meta-modeling and non-sorting genetic algorithm (NSGA II) for the patch piezoelectric and blocked dielectric constants automatic evaluations for the different identifiable behaviors by minimizing measured and computed open-circuit frequencies deviations for first 8 modes. The proposed procedure robustness comes from handling the design parameters uncertainties as large margin variations from the completed manufacturer's generic data.

The present investigations have shown that the bonded piezoceramic patch has piezoelectric

and dielectric effective *orthotropic* behaviors which are dominated by the piezoelectric transverse response mode's *four* (3 piezoelectric, 1 dielectric) constants only according to the sensitivities analyses. The latter showed also that the identification procedure analyses can be reduced to the electromechanically coupled modes only; therefore, when combining these two advantages, the resulting piezoelectric and dielectric behaviors were found to be *transverse isotropic*.

It's worthy to recall that these original new results were reached thanks to the combination of the proposed new features for the identification of piezoelectric bonded patches electromechanical properties compared to the current state of the art of this topic: (i) 3D quadratic (20 nodes) FE for modeling both the host plate and the patch in order to avoid the non-negligible models kinematics assumptions influence, (ii) response surface methodology (RSM)-based sensitivity analyses in order to investigate computational gains from potential design parameters reduction by keeping only the dominant ones, and for meta-modeling, (iii) RSM-induced polynomial meta-models use, instead of FE, for saving computation time during the NSGA II optimization process, (iv) frequencies multiple (multi-objective) deviations use and not the latters' modal sum (single-objective), (v) uncertain initial piezoelectric and dielectric piezoceramic materials constants through a realistic variation margin of +/-20% as informed by manufacturers websites in order to reach a robust identification, (vi) considering all materials' behaviors possibilities (orthotropic, transverse isotropic) for identifying the materials effective behaviors without making a priori assumptions.

## Acknowledgments

Support of the first author from the Comet-K2 Austrian Centre of Competence in Mechatronics (ACCM) at Linz (Austria) is gratefully acknowledged.

## References

- Araujo, A.L., Lopes, H.M.R., Vaz, M.A.P., Mota Soares, C.M., Herskovits, J. and Pedersen, P. (2006), "Parameter estimation in active plate structures", *Comput. Struct.*, **84**(22-23), 1471-1479.
- Araujo, A.L., Mota Soares, C.M., Friedmann, H., Röhner, J. and Henkel, F.O. (2009), "Optimal location of piezoelectric patches and identification of material properties in laminated composite structures", *Proceedings of the 4th ECCOMAS Thematic Conference on Smart Structures and Materials*, Porto, Portugal, 13-15 July.
- Araujo, A.L., Mota Soares, C.M., Herskovits, J. and Pedersen, P. (2002), "Development of a finite element model for the identification of mechanical and piezoelectric properties through gradient and experimental data", *Compos. Struct.*, **58**(3), 307-318.
- Araujo, A.L., Mota Soares, C.M., Herskovits, J. and Pedersen, P. (2009), "Estimation of piezoelectric and viscoelastic properties in laminated structures", *Compos. Struct.*, **87**(2), 168-174.
- Araujo, A.L., Mota Soares, C.M., Herskovits, J. and Pedersen, P. (2010), "Inverse techniques for the characterization of mechanical and piezoelectric properties of composite and adaptive structures: a survey", *Computational Technology Reviews*, **2**, 103-123, doi:10.4203/ctr.2.5.
- Battaglia, G.J. and Maynard, J.M. (1996), "Mean square error: a useful tool for statistical process management", *AMP J. Tech.*, **34**, 1256-1260.
- Batzmaz, I. and Tunali, S. (2003), "Small response surface designs for meta-model estimation", *Eur. J. Oper. Res.*, **145**, 455-470.
- Benjeddou, A. (2009), "New insights in piezoelectric free-vibrations using simplified modeling and

- analyses”, *Smart Struct. Syst.*, **5**(6), 591-612.
- Benjeddou, A. (2010), “Approximate evaluation of the modal effective electromechanical coupling coefficient”, *Proceedings of the IUTAM Symposium on Multifunctional Material Structures and Systems*, (Eds., B. Dattaguru, S. Gopalakrishnan and V.K. Aatre), Springer, Dordrecht.
- Chevallier, G. and Benjeddou, A. (2009), “Effective electromechanical coupling in piezoelectric composite structures” (in French), *Rev. Compos. Matér. Av.*, **19**(3), 339-364.
- Chevallier, G., Ghorbel, S. and Benjeddou, A. (2008), “A benchmark for free vibration and effective coupling of thick piezoelectric smart structures”, *Smart Mater. Struct.*, **17**(6), 065007.
- Deb, K. (2007), “Current trends in evolutionary multi-objective optimization”, *Int. J. Simul. Multidisci. Des. Optim.*, **1**(1), 1-8.
- Deb, K., Pratep, A., Agrawal, S. and Meyarivan, T. (2002), “A fast and elitist multi-objective genetic algorithm: NSGA-II”, *IEEE T. Evolut. Comput.*, **6**(2), 182-197.
- Hamdi, M., Ghanmi, S., Benjeddou, A. and Nasri, R. (2010), “Multi-objective optimization-based identification of the three dimensional elastic behavior of a multilayer composite” (in French), *Proceedings of the 1<sup>st</sup> Conference on Passive and Active Mechanical Innovations in Analysis & Design of Mechanical Systems*, Djerba, Tunisia, 22-24 March.
- Hamdi, M., Ghanmi, S., Benjeddou, A. and Nasri, R. (2012), “Simulation-test frequency updating-based inverse identification of the three dimensional elastic behavior of a piezoceramic patch bonded to a composite plate” (in French), *Proceedings of the 2nd Tunisian Congress on Mechanics*, Sousse, Tunisia, 19-21 March.
- Hamdi, M., Ghanmi, S., Benjeddou, A. and Nasri, R. (2013), “Robust electromechanical finite element updating for piezoelectric structures effective coupling prediction”, *J. Intel. Mat. Syst. Struct.*, DOI: 10.1177/1045389X13484099.
- Montemurro, M., Nasser, H., Koutsawa, Y., Belouettar, S., Vincinti, A. and Vannucci, P. (2012), “Identification of electromechanical properties of piezoelectric structures through evolutionary optimization techniques”, *Int. J. Solids Struct.*, **49**(13), 1884-1892.
- Myers, R.H. and Montgomery, D.C. (2002), *Response surface methodology*, 2<sup>nd</sup> Ed, Wiley, New York.
- Wesolowski, M. and Barkanov, E. (2012), “Model errors influence on identified composite materials properties”, *Compos. Struct.*, **94**(9), 2716-2723.

## Appendix A

The 8 OC modes electric potential distributions, computed using nominal data of Table 1, are as in Fig. 7. The electromechanically coupled modes can be recognized by the VOLT SMX values; higher the latter are higher the effective modal electromechanical coupling is.

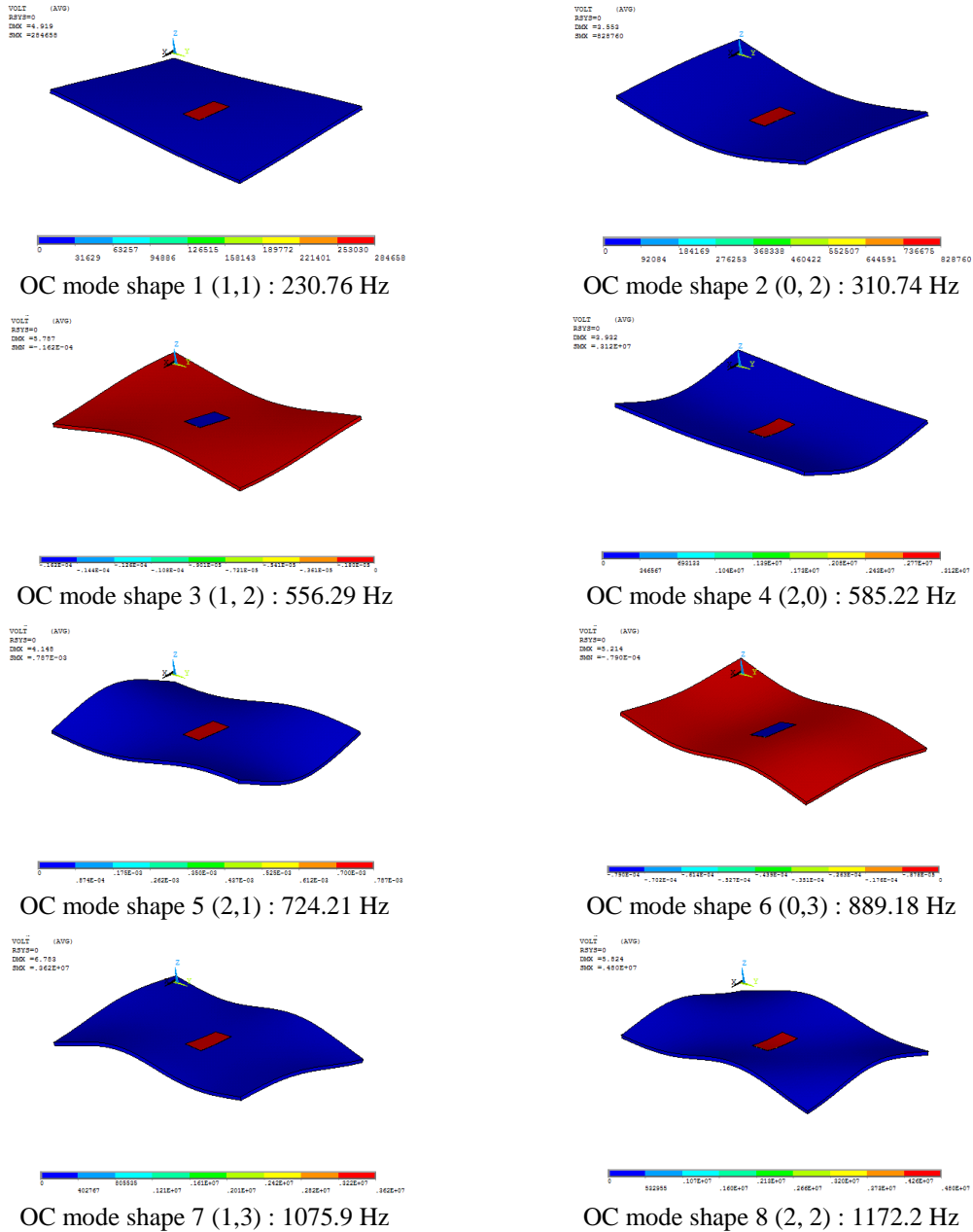


Fig. 7 Free piezoelectric adaptive plate's 8 first modes electric potential distributions

## Appendix B

The numerical designs complete factorial plan of size  $2^5=32$  for the transverse–isotropic behavior sensitivity analysis and RSM meta–modeling is given in Table 17. Notice that this behavior’s symmetry relations, as given in Eq. (7), are coded within the designs plan.

Table 17 Designs complete factorial plan for the piezoelectric and dielectric transverse-isotropic behavior analyses

Design	Non-dimensional parameters*					Numerical (FE computed) OC frequencies (Hz)							
	N°	$x_1$	$x_2$	$x_3$	$x_4$	$x_5$	F <sub>1</sub>	F <sub>2</sub>	F <sub>3</sub>	F <sub>4</sub>	F <sub>5</sub>	F <sub>6</sub>	F <sub>7</sub>
1	-1	-1	-1	-1	-1	230.79	310.90	556.29	586.45	724.21	889.18	1076.8	1173.7
2	1	-1	-1	-1	-1	230.77	310.74	556.29	585.25	724.21	889.18	1075.9	1172.3
3	-1	1	-1	-1	-1	230.77	310.75	556.29	585.29	724.21	889.18	1075.9	1172.3
4	1	1	-1	-1	-1	230.75	310.63	556.29	584.46	724.21	889.18	1075.3	1171.3
5	-1	-1	1	-1	-1	230.79	310.90	556.29	586.46	724.21	889.18	1076.8	1173.7
6	1	-1	1	-1	-1	230.77	310.74	556.29	585.26	724.21	889.18	1075.9	1172.3
7	-1	1	1	-1	-1	230.77	310.75	556.29	585.29	724.21	889.18	1075.9	1172.3
8	1	1	1	-1	-1	230.75	310.64	556.29	584.46	724.21	889.18	1075.3	1171.3
9	-1	-1	-1	1	-1	230.79	310.90	556.29	586.45	724.21	889.18	1076.8	1173.7
10	1	-1	-1	1	-1	230.77	310.74	556.29	585.25	724.21	889.18	1075.9	1172.3
11	-1	1	-1	1	-1	230.77	310.75	556.29	585.29	724.21	889.18	1075.9	1172.3
12	1	1	-1	1	-1	230.75	310.63	556.29	584.46	724.21	889.18	1075.3	1171.3
13	-1	-1	1	1	-1	230.79	310.90	556.29	586.46	724.21	889.18	1076.8	1173.7
14	1	-1	1	1	-1	230.77	310.74	556.29	585.26	724.21	889.18	1075.9	1172.3
15	-1	1	1	1	-1	230.77	310.75	556.29	585.29	724.21	889.18	1075.9	1172.3
16	1	1	1	1	-1	230.75	310.64	556.29	584.46	724.21	889.18	1075.3	1171.3
17	-1	-1	-1	-1	1	230.79	310.90	556.29	586.41	724.21	889.18	1076.7	1173.7
18	1	-1	-1	-1	1	230.76	310.74	556.29	585.22	724.21	889.18	1075.9	1172.2
19	-1	1	-1	-1	1	230.77	310.74	556.29	585.27	724.21	889.18	1075.9	1172.3
20	1	1	-1	-1	1	230.75	310.63	556.29	584.45	724.21	889.18	1075.3	1171.3
21	-1	-1	1	-1	1	230.79	310.90	556.29	586.41	724.21	889.18	1076.7	1173.7
22	1	-1	1	-1	1	230.76	310.74	556.29	585.22	724.21	889.18	1075.9	1172.2
23	-1	1	1	-1	1	230.77	310.74	556.29	585.27	724.21	889.18	1075.9	1172.3
24	1	1	1	-1	1	230.75	310.63	556.29	584.45	724.21	889.18	1075.3	1171.3
25	-1	-1	-1	1	1	230.79	310.90	556.29	586.41	724.21	889.18	1076.7	1173.7
26	1	-1	-1	1	1	230.76	310.74	556.29	585.22	724.21	889.18	1075.9	1172.2
27	-1	1	-1	1	1	230.77	310.74	556.29	585.27	724.21	889.18	1075.9	1172.3
28	1	1	-1	1	1	230.75	310.63	556.29	584.45	724.21	889.18	1075.3	1171.3
29	-1	-1	1	1	1	230.79	310.90	556.29	586.41	724.21	889.18	1076.7	1173.7
30	1	-1	1	1	1	230.76	310.74	556.29	585.22	724.21	889.18	1075.9	1172.2
31	-1	1	1	1	1	230.77	310.74	556.29	585.27	724.21	889.18	1075.9	1172.3
32	1	1	1	1	1	230.75	310.63	556.29	584.45	724.21	889.18	1075.3	1171.3

\*  $x_1 = e_{31} = e_{32}$ ,  $x_2 = e_{33}$ ,  $x_3 = e_{15} = e_{24}$ ,  $x_4 = \epsilon_{11}^S = \epsilon_{22}^S$ ,  $x_5 = \epsilon_{33}^S$

The numerical designs complete factorial plan of size  $2^4=16$  for the influent parameters– based orthotropic behavior sensitivity analysis and RSM meta–modeling is as in Table 18.

Table 18 Designs plan for influent parameters–based piezoelectric and dielectric orthotropic behavior analyses

Design	Non-dimensional parameters*				Numerical (FE computed) OC frequencies (Hz)							
	N <sup>o</sup>	x <sub>1</sub>	x <sub>2</sub>	x <sub>3</sub>	x <sub>4</sub>	F <sub>1</sub>	F <sub>2</sub>	F <sub>3</sub>	F <sub>4</sub>	F <sub>5</sub>	F <sub>6</sub>	F <sub>7</sub>
1	-1	-1	-1	-1	230.79	310.90	556.29	586.45	724.21	889.18	1076.8	1173.7
2	1	-1	-1	-1	230.78	311.09	556.29	585.05	724.21	889.18	1076.1	1172.4
3	-1	1	-1	-1	230.78	310.60	556.29	586.75	724.21	889.18	1076.6	1173.7
4	1	1	-1	-1	230.77	310.74	556.29	585.25	724.21	889.18	1075.9	1172.3
5	-1	-1	1	-1	230.77	310.75	556.29	585.29	724.21	889.18	1075.9	1172.3
6	1	-1	1	-1	230.76	310.86	556.29	584.37	724.21	889.18	1075.5	1171.4
7	-1	1	1	-1	230.76	310.55	556.29	585.41	724.21	889.18	1075.8	1172.2
8	1	1	1	-1	230.75	310.63	556.29	584.46	724.21	889.18	1075.3	1171.3
9	-1	-1	-1	1	230.79	310.90	556.29	586.41	724.21	889.18	1076.7	1173.7
10	1	-1	-1	1	230.78	311.09	556.29	585.02	724.21	889.18	1076.1	1172.3
11	-1	1	-1	1	230.78	310.60	556.29	586.70	724.21	889.18	1076.6	1173.6
12	1	1	-1	1	230.76	310.74	556.29	585.22	724.21	889.18	1075.9	1172.2
13	-1	-1	1	1	230.77	310.74	556.29	585.27	724.21	889.18	1075.9	1172.3
14	1	-1	1	1	230.76	310.85	556.29	584.36	724.21	889.18	1075.5	1171.4
15	-1	1	1	1	230.76	310.55	556.29	585.39	724.21	889.18	1075.8	1172.2
16	1	1	1	1	230.75	310.63	556.29	584.45	724.21	889.18	1075.3	1171.3

\*  $x_1 = e_{31}, x_2 = e_{32}, x_3 = e_{33}, x_4 = \epsilon_{33}$ ; other 4 parameters of the orthotropic behavior remain in their nominal values during the 3D FE simulations

The numerical designs complete factorial plan of size  $2^3=8$  for the influent parameters– based transverse–isotropic behavior sensitivity analysis and RSM meta–modeling is given in Table 19. The symmetry relations, as in Eq. (7), are also coded within the designs plan.

Table 19 Designs plan for influent parameters–based piezoelectric and dielectric transverse–isotropic behavior analyses

Design	Non-dimensional parameters*			Numerical (FE computed) OC frequencies (Hz)							
	N <sup>o</sup>	x <sub>1</sub>	x <sub>2</sub>	x <sub>3</sub>	F <sub>1</sub>	F <sub>2</sub>	F <sub>3</sub>	F <sub>4</sub>	F <sub>5</sub>	F <sub>6</sub>	F <sub>7</sub>
1	-1	-1	-1	230.79	310.90	556.29	586.45	724.21	889.18	1076.8	1173.7
2	1	-1	-1	230.77	310.74	556.29	585.25	724.21	889.18	1075.9	1172.3
3	-1	1	-1	230.77	310.75	556.29	585.29	724.21	889.18	1075.9	1172.3
4	1	1	-1	230.75	310.63	556.29	584.46	724.21	889.18	1075.3	1171.3
5	-1	-1	1	230.79	310.90	556.29	586.41	724.21	889.18	1076.7	1173.7
6	1	-1	1	230.76	310.74	556.29	585.22	724.21	889.18	1075.9	1172.2
7	-1	1	1	230.77	310.74	556.29	585.27	724.21	889.18	1075.9	1172.3
8	1	1	1	230.75	310.63	556.29	584.45	724.21	889.18	1075.3	1171.3

\*  $x_1 = e_{31} = e_{32}, x_2 = e_{33}, x_3 = \epsilon_{33}$ ; other 2 parameters of the transverse – isotropic behavior remain in their nominal values during the 3D FE simulations